공학석사학위논문

기울어진 벽과 충돌하는 상승 기포 역학에 대한 실험적 연구

Experimental study of dynamics of a rising bubble impacting on the inclined wall

2023년 2월

서울대학교 대학원

기계공학부

최 진 용

기울어진 벽과 충돌하는 상승 기포 역학에 대한 실험적 연구

Experimental study of dynamics of a rising bubble impacting on the inclined wall

지도교수 박 형 민

이 논문을 공학석사 학위논문으로 제출함

2022년 10월

서울대학교 대학원
기계공학부
최 진 용

최진용의 석사 학위논문을 인준함

2022년 12월

위 원 장 김 호 영 (인)

부위원장 박 형 민 (인)

위 원 황 원 태 (인)

Experimental study of dynamics of a rising bubble impacting on the inclined wall

Jinyong Choi
Department of Mechanical Engineering
Seoul National University

Abstract

In the present study, we experimentally investigated the dynamics of a single rising air bubble, which diameter is in range of 2-3mm and having two dimensional ellipsoid shape, (Reynolds numbers in the order of 10^2 and Weber number in the range of 3-4) impacting on the inclined wall installed on top of the static acrylic tank containing room temperature tap water. While varying the material of the wall (e.g., PMMA and glass) and the inclination angle of the wall from 5° to 85° with an interval of 5°, we measured trajectory of the bubble centroid and shape deformation of the bubble surface using high-speed shadowgraphy and observed evolution of the liquid flow field near the bubble and the wall with two-phase particle image velocimetry (PIV) technique. After some initial collisions with the wall, the bubble either slides parallel to the wall or bounces against the wall repeatedly. By comparing the values of wall perpendicular directional and wall parallel directional forces acting on the bubble at the moment of collision,

transition mechanism of the bubble dynamics is explained. We verified that the transition condition of the bubble behavior in high Weber number is solely determined by the inclination angle of the wall, regardless of the wall boundary condition (i.e., material of the wall). Transition of the bubble dynamics occurs when the wall repulsive force, which is mainly originated by the pressure difference between the thin film of liquid near the wall and the deformed bubble, is balanced with the buoyancy of the bubble that acts as the wall attraction force. We suggest that surface tension force, which is usually considered negligible in previous studies, also derives the bubble to move away from the wall and should be taken into consideration when giving detailed explanation about the transition mechanism. We also discussed the effect of the wall boundary condition (i.e., wettability of the wall) by analyzing trajectory of the bubble centroid with fitted trigonometric equation, observing change of period and amplitude of the periodical rebounds. The effect of different wall boundary condition, which is found to affect the area of region where the force exerted by the wall is dominant, is apparent only when the inclination angle of the wall is far more higher than the transition angle. We also looked at the spatio-temporal evolution of the liquid flow field around the bubble at the instant of bubble-wall collision to explain the different bubble-wall interaction mechanism before and after the transition has occurred. With all the experimental results and discussions combined, future study regarding various wall

boundary conditions, such as porous, superhydrophobic and superhydrophilic wall, is proposed and the efficacy of the application of the multiphase flow such as bubbly flow in industrial applications is suggested.

Keyword : rising bubble, wettability, shadowgraphy, two-phase particle image velocimetry, surface tension

Student Number : 2021-22293

To my father for his unconditional love

Table of Contents

Abstract ····· i
Table of Contents ····· v
List of Tables ····· vii
List of Figures ····· viii

Chapter
1. Introduction ····· 1

2. Experimental set-up and procedure ····· 6
2.1. Single bubble rising near an inclined wall ····· 6
2.2. High-speed shadowgraphy ····· 8
2.3. Two-phase particle image velocimetry ····· 9

3. Results and discussions ····· 15
3.1. Bubble behavior regime classification ····· 15
3.2. Trajectory of the bubble at bouncing regime ····· 19
3.3. Force scaling analysis ····· 20
3.4. Energy Method ····· 25

4. Conclusions ····· 37

Bibliography ····· 39

Abstract in Korean ····· 42

List of Tables

Table 2.1. Nondimensionalized variables and its units ····· 11

Table 3.1. Constants of sine fitted equations, PMMA wall ····· 27

Table 3.2. Constants of sine fitted equations, glass wall ····· 28

List of Figures

Figure 2.1. (a) Schematic diagram of the experimental setup for the water tank installed with inclined wall for the two-phase PIV (particle image velocimetry) with syringe pump, high speed camera and CW laser (b) Maagnified schematic diagram for defining the bubble kinematic variables (c) Raw image of the water droplet on the PMMA wall ····· 12

Figure 2.2. (a) Raw image (b) superimposed image of bubble image at inclination angle of 15°, PMMA wall (c) PIV raw image at inclination angle of 30°, PMMA wall ····· 13

Figure 2.3. Normalized (a) trajectory of the bubble centroid (b) aspect ratio (c) distance from the bubble centroid to the wall at 15°, PMMA wall ····· 14

Figure 3.1. Superimposed bubble edge image at the inclination angle of the wall of (a) 10°, (c) 30° , (d) 45° at PMMA wall, (b) Magnified view of red squared area in (a) ····· 29

Figure 3.2. (a) Total speed (b) x-directional speed (c) y-directional speed of the bubble centroid at the inclination angle of 15°, PMMA wall (d) Aspect ratio of the bubble at the inclination angle of 15°, PMMA wall ····· 30

Figure 3.3. (a) Total speed (b) x-directional speed (c) y-directional speed of the bubble centroid at the inclination angle of 30°, PMMA wall (d) Aspect ratio of the bubble at the inclination angle of 30°, PMMA wall ····· 31

Figure 3.4. Superimposed image of the bubble impacting on the (a) glass (b) PMMA wall, at the inclination angle of the wall of 45° ····· 32

Figure 3.5. Non-dimensionalized velocity of the bubble bouncing with the (a) PMMA (b) glass wall of inclination angle of 45° ····· 33

Figure 3.6. Vortex pair structure behind the bubble at the inclination angle of (a) sliding regime (b) bouncing regime ···· ····· 34

Figure 3.7. Forces that act on the bubble with the inclination angle of (a) 40°, (b) 45° of PMMA wall ····· 35

Figure 3.8. Ratio of kinetic energy to total energy value, ratio of surface tension energy to total energy value, total energy value, aspect ratio of the bubble at the inclination angle of (a) 20°, (b) 45°, (c) 80° of PMMA wall ····· 36

Chapter 1.
Introduction

Rising bubbles interacting with various conFigureurations of walls are easily found in lots of natural phenomena and various industrial applications. Some examples of these implementations could be wastewater treatment plants (WWTP) such as flocculation plants, where the bubbles are generated on purpose in order to entrain and remove unwanted minerals or plastic particles from the wastewater, and small modular nuclear reactors (SMRs) placed at shaking ships for the marine propulsion where the bubble generation is unprofitable yet unavoidable. In this sense, understanding of the mechanism of the bubble-wall interaction will not only enhance the efficiency of the system (Sol et al., 2020), but also ensure the safe operation of the system (Hirdaris et al., 2014). Furthermore, understanding of the bubble-wall interaction mechanism is not only function as a technological leap for the engineering applications but also function as a basic prior knowledge for researching multiphase flow interacting with surfaces of various compositions and complex structures. Therefore, needs for the elaborated understanding of the effect of wall presence on the rising bubble is arising for both academic and practical backgrounds. Yet, despite of the simplicity of the problem settings that no cumbersome external force is exerted to the air bubble except buoyancy (i.e. gravity), knowledge about the mechanism of the interaction between the buoyancy-driven rising bubble and the wall, and change of the bubble dynamics due to the presence of the wall is not yet complete.

In this context, many researchers have been studying the effects of vertical or horizontal walls on the rising bubble dynamics. Jeong and Park, 2015 conducted an experiment with a single bubble rising near the vertical wall with various wall compositions, such as superhydrophobic, superhydrophilic and porous wall. They explained the effect of the wall presence to the bubble dynamics by focusing on the interchange and balance between kinetic energy and surface tension energy of the bubble, and discovered that the wall effect is highly subjective to the proximity of the bubble centroid to the wall. They also showed that the effect of the wall presence could be considerably altered with the choice of different composition of the wall. Maeng and Park, 2021 used shadowgraphy with high-speed camera and two-phase particle image velocimetry (PIV) technique to measure the variation of the wall-Nusselt number and heat transfer coefficient in the setup of a single bubble rising near the heated vertical wall. They showed that the heat transfer of the wall could be dramatically increased owing to the mixing effect caused by the inertial wake of the rising bubble. These researches proposed the practical applicability and efficacy of employing bubble-wall interactions in industrial applications, but these researches have limitations in that their scopes are only confined to vertical or horizontal wall conFigureurations. Problem associated with the inclined wall, at which the bubble dynamics is apt to switch its characteristics with just a subtle change of the inclination angle of the wall, is a much more complex problem to solve.

Therefore, research on the behavior of rising bubbles near inclined walls has also been actively conducted recently. Barbosa et al, 2016 experimentally investigated the kinetic behavior of different sized bubbles rising in various quiescent liquids near an inclined wall. They

classified the motion of the bubble as two main categories: one is constant-speed sliding motion parallel to the wall direction and the other is periodic bouncing motion against the wall while rising. By means of force-scaling analysis, they showed that each case of the experimental set-ups has different transition angles, which is defined as an value of the inclination angle of the wall when the wall repulsive force that pushes the bubble away from the wall is same or higher than the buoyancy of the bubble that keeps the bubble arise near to the wall. Thus at angle larger than the transition angle the bubble does not attach to the wall anymore and bounces off from the wall. This means that the type of liquid and the size of the bubble affects the interactions between the bubble and the wall. They also observed that the wall repulsive force, which originates from the breakdown of the inertial wake structure behind the bubble, is a function of the bubble Weber number. Based on these observations, they concluded that the transition angle can be determined by only measuring the bubble Weber number-wall repulsive force is dependent to it-and the bubble Reynolds number-buoyancy is dependent to it. This result has been a starting point for the many subsequent researches that focus on the bubble-wall interactions. Lots of numerical analysis researches, which become a lot more effective by the rapid development of computing power recently, suggested various numerical models for the wall repulsive force and the bubble-wall interactions to match and imitate the transition condition proposed by experiments. They were successful to reproduce the experimental result of the bubble's kinematic behaviors such as shape deformation and periodical trajectory of the bubble centroid. (Khodadadi et al., 2022; Javadi et al., 2018)

However, since most of the previous researches, both experimental

and numerical studies, are still limited to the dynamics of small to moderate Weber and Reynolds number bubbles. This setting corresponds to the problem of rising small spherical bubbles, which is not so much frequent in actual engineering applications. Therefore, the dynamics of higher Reynolds and Weber number bubbles interacting with the inclined wall, which corresponds to the case of ellipsoidal rising bubbles that can be seen more frequently in industrial applications, remains as an unsolved problem. Furthermore, despite the fact that the effect of different wall boundary condition is proved to considerably change the bubble dynamics (Jeong and Park, 2015), the wall boundary condition is not fully considered in previous studies also. Therefore, problem of the dynamics of a rising bubble with a high Weber and Reynolds number under the different wall boundary conditions remains as an important and unsolved problem.

With the consideration of these challenges presented, we aim the purpose of this study to experimentally investigate the dynamics of a single rising bubble with a high Reynolds (order of 10^2) and Weber (range of 3-4) number impacting on the inclined wall with two different materials, which is PMMA and glass, while changing the inclination angle of the wall to characterize the effects of both the wall material and the inclination angle of the wall on the dynamics of a single rising bubble. We measure the bubble's kinematic properties such as velocity of the bubble centroid, two dimensional equivalent diameter and aspect ratio of the bubble, and distance from the bubble centroid to the wall with high-speed shadowgraphy to match the experimental results with previous studies. We also suggest the general explanations about the transition mechanism of the bubble dynamics by conducting force scaling analysis using novel approach, and that explanation is reasonable to the larger-sized bubble as well

as the small bubble that have been studied earlier. By comparing the experimental results carried out with PMMA wall set-up with these of glass wall set-up, we will also explain the effect of wall boundary condition to the bubble-wall interactions. We will assert that the surface tension force, which has been frequently neglected in force scaling analysis, should be considered and has predominant effect on the transition. Periodicity of repeated bouncing motion, which is observed after the transition of the bubble behavior from sliding to bouncing, is analyzed by looking at the change of total energy value-defined by the sum of the kinetic energy and the surface tension energy of the bubble-in amid of the bubble-wall collision. We will also look at the spatio-temporal evolution of the liquid flow field acquired by two-phase particle image velocimetry to explain the mechanism of repulsive force that has acted by the wall. With all these results and discussions, profound understanding about the bubble-wall interaction and transition mechanism of the bubble dynamics will become possible.

Chapter 2.
Experimental set-up and procedure

2.1. Single bubble rising near an inclined wall

The experiments are conducted in a static water tank made of acryl, of which has the dimensions of $400\times1000\times300mm^3$ along the transverse (x), longitudinal (y) and depth (z) directions respectively. The water tank contains half the volume of tank with room temperature (25℃) tap water [Figure 2.1. (a)]. Behind the water tank, a LED backlight panel is fixated to provide a light source. A 20-gauge needle, which inner diameter has the dimension of 0.603mm, is installed at 20mm height from the floor of the tank and pushed gently by a syringe pump (Fusion 100-X Touch, Chemyx Inc.), with a rate of 0.02ml/min to create a single bubble. The needle tip is inserted deep enough (needle penetration length has order 100 times higher than the bubble's diameter) to minimize the influence of the side wall of the tank. Each experiments are conducted one after another with sufficient time interval to ensure that the effect of the precedent bubble and its wake has sufficiently decayed. 5mm thick wall with different materials (PMMA and glass) is held by a free-stop hinge, set 150mm above the needle tip with the fishing wire connected to the hinge, to incline the wall by a desired angle. Measured contact angle of the two walls were 57.57° for the PMMA wall, and 23.24° for the glass wall, which is consistent with a small error with previous studies. (Ngai et al., 2017; Winandy et al., 2018) [Figure 2.1. (c)] The inclination angle of the wall is varied from 5° to

85°, with an interval of 5° (error of ±1°). High-speed camera (NX5, Integrated Design Tools Inc.) is set perpendicular to the plane where the bubble moves and collision between the bubble and the wall occurs (xy plane), and also perpendicular to the green laser sheet in order to conduct shadowgraphy and two-phase PIV techniques [Figure 2.1. (a)].

First, the behavior and dynamic characteristics of an undisturbed single rising bubble are captured by conducting high-speed (500 fps) shadowgraphy in an unbounded state. In an unbounded state, the inclined walls are removed from the tank so that the bubble can freely rise without the influence of boundaries such as the wall. We repeat this unbounded experiment three times to confirm the reliability and repeatability of the experiment. Averaged values of repeated experiments are set as reference bubble dynamics value, which is a reference value for comparison with disturbed, or the wall-bounded bubble experiment results. The unbounded bubble rose along the water in xy plane with a zigzag path without any z coordinate deviation, so we can assume that the kinematic properties of the bubble is two dimensional, i.e., there is no z directional speed. The unbounded bubble showed shape of an z-axis axisymmetric ellipsoid, of which average bubble equivalent diameter ($d_{eq,0}$) is $d_{eq,0} = (d_{maj}^2 d_{\min})^{(1/3)} = 2.48mm(\pm 0.01mm)$, where d_{maj} and $d_{\min}$ are the length of the major and minor axis of the ellipsoidal bubble projected to xy plane respectively. Average aspect ratio of the bubble (χ_0) is $\chi_0 = d_{maj}/d_{\min} = 2.2(\pm 0.1)$ [Figure 2.1. (b)]. Average terminal rising velocity of the bubble (U_0), which is defined as the velocity of the bubble after the bubble has reached constant rising velocity, is $U_0 = 31.31cm/s(\pm 0.01cm/s)$. We derived the characteristic time scale (τ) by dividing the average bubble diameter with average terminal

rising velocity of the bubble, $\tau = d_{eq,0}/U_0$, resulting a value of 0.0079 seconds. Reynolds number (Re) and Weber (We) number based on these kinematic properties are calculated as Re = 774.63 and We = 3.34 each. This result shows great agreement with previous studies on the bubble dynamics of a two dimensional zigzag path bubble, so we can say that our experimental set-up is generating ellipsoidal bubble rising in two-dimensional zigzag path in comparatively pure-water like condition (Lee and Park, 2017; Haberman and Morton, 1953).

With the unbounded (free) bubble kinematic properties, we nondimensionalize the kinematic variables of the bounded experimental results. Cartesian coordinates of x, y axis are normalized as $x^* = x/d_{eq,0}$ and $y^* = y/d_{eq,0}$ respectively, and normalized velocities are expressed as $U^* = U/U_0$, $u^* = u/U_0$, $v^* = v/U_0$ for total, x-directional and y-directional velocities each. Also, equivalent diameter and the distance from the bubble centroid to the wall is expressed as $d_{eq}^* = d_{eq}/d_{eq,0}$ and $s^* = s/d_{eq,0}$. For the time-relevant term, all time scales are also normalized with non-dimensionaliezd time scale of the bubble τ, $t^* = t/\tau$ [Table 2.1.].

2.2. High-speed shadowgraphy

To measure the kinematic properties of the air bubble with the presence of the wall, we use high-speed shadowgraphy image technique with white light LED panel. Images of shadow that are created by the bubble are captured by 500 fps using high speed camera. Applying some of the image processing technique present, we separate edge image of the bubble from the raw image. First, we capture background image, which is an image of water tank without

the bubble, and binarize its pixel value using certain threshold. Pixel values of this background image is set as a reference value. By subtracting pixel values of background image from the binarized bubble image, we get non-zero values for the area where the bubble edge lays on and zero values for the area where the bubble does not exist. These region of having non-zero values is considered as bubble edge, and by filling the hole inside the bubble edge image we can get a total bulk image of bubble. With this processed bubble image, we also superimpose individual frames of the bubble edge image with an interval of 3 frames (0.003 sec) to make it easy to see the trajectory and behavior of the bubble by looking at a single image [Figure 2.2. (a), (b)]. By analyzing the characteristics of the bubble image frame by frame, measuring bubble's kinematic properties such as aspect ratio, equivalent diameter, velocity, and the like is possible [Figure 2.3. (a), (b), (c)].

2.3. Two-phase particle image velocimetry

Liquid flow field around the wall at the instant of collision is measured by adapting high-speed two-phase particle image velocimetry (PIV) technique. To track and visualize the liquid flow, we use red fluorescent PIV seeding particles (PMMA Rhodamine-B, size in range of 1-20μm). Since the seeding particles absorbs 560 nm and emits 584 nm wavelength lights, we use continuous-wave (CW) laser (RayPower 5000, Dantec Dynamics) to produce a green sheet of laser (wavelength of 532 nm) that illuminates the PIV seeding particles, and red-colored LED (wavelength of 675 nm) panel as a backlight to visualize the bubble. Orange filter (cut-off length of ~570nm, Heliopan) is installed at the front of the camera lens to

screen and filter the green laser which could be reflected from the bubble. Stokes number of the seeding particle is 6.76×10^{-4}, so we can assume that the particles have only little effect on the fluid flow and the bubble. Images of the liquid flow field are captured with a resolution of 720 × 1280 pixels, 1000 frames per second [Figure 2.2. (c)]. Applying same binarization method used in high-speed shadowgraphy and additionally appling LoG (Log of Gaussian) filter, which eliminates small objects (particles) in an image, to the background image, we are able to distinguish the particle image from the background image. Velocity vectors are calculated from the particle image by using cross-correlation using FFT (fast Fourier transform) algorithm, with interrogation window size of 32 × 32 pixel and 50% overlap ratio. Interval between each vector is 8 pixels, which is about 0.26 mm in real scale (Lee and Park, 2017; Lindken and Merzkirch, 2002).

Variables (Unit)	Non-dimensionalized form
Diameter (mm)	$d^* = d/d_{eq,0}$
Time (sec)	$t^* = t/\tau$
X-coordinate (mm)	$x^* = x/d_{eq,0}$
Y-coordinate (mm)	$y^* = y/d_{eq,0}$
Distance to the wall (mm)	$s^* = s/d_{eq,0}$
Total velocity (cm/s)	$U^* = U/U_0$
X-directional velocity (cm/s)	$u^* = u/U_0$
Y-directional velocity (cm/s)	$v^* = v/U_0$
Aspect ratio	$\chi = d_{\max}/d_{\min}$

Table 2.1. Nondimensionalized variables and its units

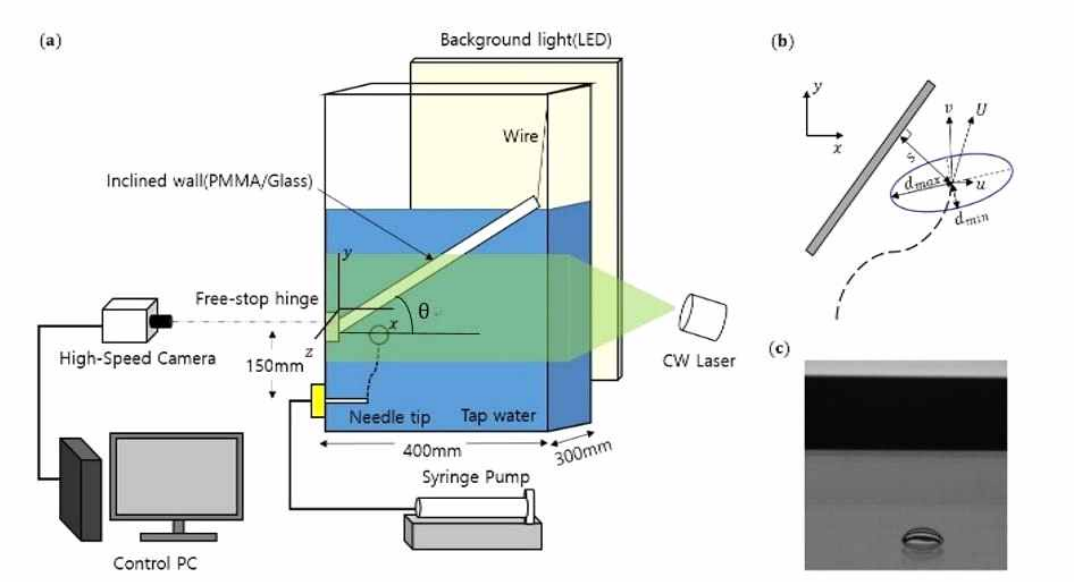

Figure 2.1. (a) Schematic diagram of the experimental setup for the water tank installed with inclined wall for the two-phase PIV (particle image velocimetry) with syringe pump, high speed camera and CW laser (b) Maagnified schematic diagram for defining the bubble kinematic variables (c) Raw image of the water droplet on the PMMA wall

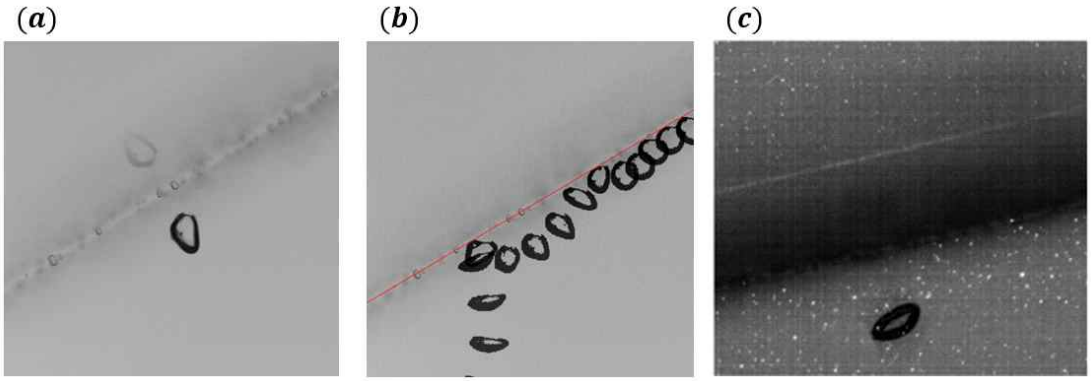

Figure 2.2. (a) Raw image (b) superimposed image of bubble image at inclination angle of 30°, PMMA wall (c) PIV raw image at inclination angle of 15°, PMMA wall

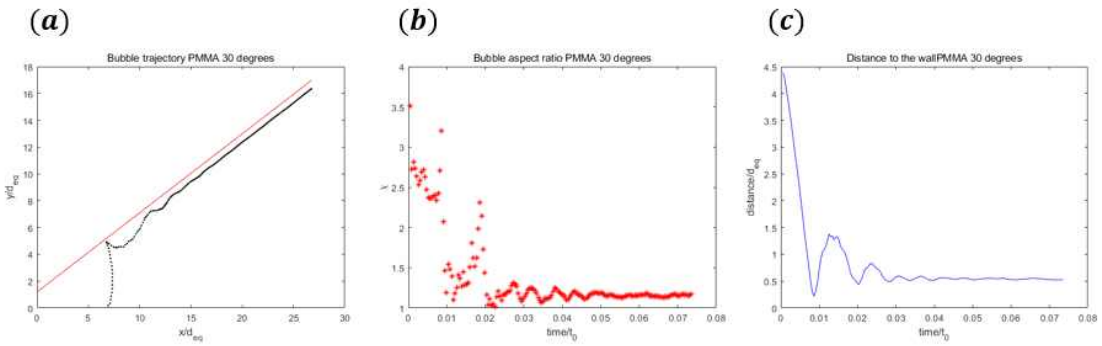

Figure 2.3. Normalized (a) trajectory of the bubble centroid (b) aspect ratio (c) distance from the bubble centroid to the wall at 30°, PMMA wall

Chapter 3.
Results and discussions

3.1. Bubble behavior regime classification

Behavior of the rising bubble interacting with the inclined wall can be divided into three main categories: 1. sliding along the wall accompanied by shape oscillation, 2. sliding along the wall without shape oscillation, 3. periodic repeated bouncing against the wall. From the visualization experimental results, main criterion that divides the regime of bubble behavior is observed to be the inclination angle of the wall.

First regime is when the inclination angle of the wall is 15° and lower, and in this regime motion of the bubble is characterized as sliding along the wall parallel direction, accompanied by shape oscillation [Figure. 3.1. (a)]. When the bubble gets closer to the wall, the liquid layer near the wall is pressed and tapered, and pressure of the liquid film becomes higher. This leads to the flattening of the bubble to the major axis, which results in changing the shape of the bubble to be disk-like shape. By increasing the surface area, the bubble accumulates excessive energy exerted by the pressed liquid layer in the form of surface tension energy. After the flattening, the bubble collides with the wall for the first time and subsequently violent bubble shape deformation and transverse dislocation of the bubble occurs. It is because surface tension energy accumulated at the top surface of the bubble is being dissipated by the effect of the repulsive force acted by the wall. Unlike solid particles which exhibit elastic deformation-free rebounds, surface of the bubble deforms

under external force in the process of bouncing off and this deformation acts as the main energy dissipation mechanism for the bubble. The bubble loses some of its accumulated energy through the collision, yet rise again near the wall under the influence of buoyancy and repeat this partly elastic collision few times until the steady sliding state is achieved. Consecutive bounce-offs act as a major damping source of the bubble's kinetic (and total) energy, and after few initial collisions the bubble starts to slide parallel to the wall direction. After reaching the steady sliding state, where net force perpendicular to the wall is balanced to zero, the speeds of the bubble in the x-y direction are products of the bubble's total velocity and trigonometric function values of the inclination angle, meaning that wall parallel component of buoyancy is only driving source of the bubble's motion. So it is reasonable to say that no rolling motion occurs during this steady state [Figure 3.2. (a), (b), (c)]. Detailed explanation about the energy loss in this regime will be discussed in the further chapter.

Since the inclination angle of the wall (θ) is small ($\cos\theta \gg \sin\theta$) in this regime, buoyancy force has large wall-perpendicular component ($F_B \cos\theta$) and this makes action-reaction between the bubble and the wall rampant in the wall perpendicular direction. In the process of this rigorous action-reaction, wall perpendicular directional balance of the forces are achieved quickly. Therefore, excessive surface tension energy that the bubble gained from the free rise did not completely vanish, and the bubble even gains some of the energy in the process of action-reaction with the wall. This residual energy that the bubble has not depleted thoroughly is dissipated through the shape oscillation while sliding. Fluctuation of the aspect ratio of the bubble, even after the normalized distance from the bubble centroid to the wall is

settled to steady, confirms that shape oscillation is occurring at a visible scale in this regime [Figure 3.2. (d)]. This shape oscillation is observable at raw images also [Figure 3.1. (b)].

Second regime corresponds to the region where the inclination angle of the wall is larger than 20 but smaller than 45 degrees. In this regime, the bubble slides along the wall after few initial collisions, like the first regime, but no apparent shape oscillation is observed after the steady-sliding state [Figure 3.1.(c)]. The speeds in the x-y direction are also products of the total velocity value of the bubble and trigonometric function values of the slope of the wall like the first regime, so it can be reaffirmed that even in region 2, bubble slides along the wall. Similarly to the first regime, the bubble loses its momentum and dissipates excessive accumulated surface tension energy by the means of shape deformation during the few initial collisions. However, the shape oscillation does not occur in second regime because sufficient amount of the bubble's energy was able to be damped during the initial collisions [Figure 3.3 (a), (b) (c)].

Third regime is characterized by periodic bouncing of the bubble against the wall and is observed at the inclination angle of the wall of 45 degrees and more. In this regime, even after few initial collisions that damps the total energy of the bubble, the bubble does not attach to the wall because as the inclination angle of the wall increases, dissipation of momentum that the bubble experiences during the collision, which is in wall perpendicular direction, is acting in a direction less related to effect of offsetting buoyancy. In this sense, repulsive force acted by the wall pushes the bubble away from the wall, and the bubble regains its upward momentum easily from the buoyancy and rise again, getting closer to the wall: total momentum lost during the bubble-wall collision is balanced by the

momentum that the bubble gained by buoyancy. Therefore, upward momentum is conserved after each collisions, resulting the bubble to show a series of repeated collisions periodically [Figure 3.1. (d)]. This change of the bubble behavior, from the sliding to periodic bouncing, is named as transition, and the onset of angle which the transition happens is defined as the transition angle. In this experimental set-up where the bubble equivalent diameter is in range of 2-3mm and the liquid being water, the transition angle is determined to be 45° from the previous studies (Barbosa et al., 2016, 2019). One thing that is noticeable is that changing the material of the wall from PMMA to glass does not changed the transition angle or behavior and periodicity of the bubble significantly. This might indicate that the material of the wall, or the wall boundary condition, has nothing to do with the transition mechanism. Instead, the material of the wall appears to influence contact time between the wall and the bubble, which means the time taken for the bubble to leave the wall after first contact. On PMMA wall, the bubble contacted the wall during 13 frames (0.026 sec), while on glass it was 11 frames (0.022 sec) [Figure 3.4. (a), (b)]. However, this dragging of the bubble due to the different wettability does not make any noticeable change in the bubble kinematics [Figure 3.5.]. Looking at the periodicity of the bubble motion, it is observed that the larger the inclination angle of the wall is, the bigger the values are in both amplitude and period in bouncing motion of the bubble, with little regard to the wall boundary condition.

3.2. Trajectory of the bubble at bouncing regime

Since trajectory of the bubble centroid in the bouncing regime exhibits periodic characteristics, it will be helpful to fit non-dimensionalized distance from the bubble centroid to the wall, s^* of each case to a basic periodic equation, which is sine function, to analyze its periodicity. We did fitting of the trajectory using the least square method. First, we estimate initial period and offset of the bubble trajectory from the time-averaged values of s^* and t^*. Using this value as starting point, we use fitting function engraved on computer analysis software (MATLAB R2020b, MathWorks Inc.), yielding sine curve with least squares of the residuals. General form of the fitted function is

$$s^* = C_1 \sin(C_2 t^* - C_3) + C_4, \qquad (3.1)$$

where C_1, C_2, C_3, C_4 are respectively amplitude, period, phase and offset of the sine function and these values are found to be dependent to the wall material and the inclination angle of the wall. The fitted results are shown in [Table 3.1.] and [Table 3.2.].

It is notable that there is certain threshold after which amplitude and offset of the fitted equation increases by a large margin where the period does not. It means that in this regime of large inclination angle, the bubbles had bounced off further away from the wall and get closer to the wall again, so as to say “a violent bouncing” is happening, compared to smaller inclination angle cases. In this regime, the bubble bounces off from the wall, and the reaction force of the bounce is mainly transverse (x) directional since the wall inclination angle is large that it will escape the region where the wall effect is

significant ($s^* \approx 1.5-5.0$) transversely (Jeong & Park, 2015; Zhang et al., 2019). Similar to the smaller inclination angle cases, the bubble regains momentum, which it has dissipated from the from the last collision, from the buoyancy and repeats this bouncing periodically. However, this behavior is distinctive from the periodic bouncing that can be observed at the case where inclination angle of the wall is near to the transition angle, in that in higher angles the bubble escape from the influence of the wall. Therefore, bouncing regime can be subdivided into two regimes: one being the periodic bouncing under the influence of the wall, the other to be the case in which the bubble escapes and returns to the wall effect region, thus returning to the free rise state intermittently. The threshold angle for this behavior to appear is 70° for PMMA wall and 75° for glass wall, so it is reasonable to say that the wall wettability affects magnitude of the wall effective regions. Detailed explanation by comparing change of energy values of the bubble will be discussed in further chapter.

3.3. Force scaling analysis

We performed force scaling analysis to check under which the transition of the bubble motion occurs. Forces that act on the rising bubble interacting with the wall are as follows: Basset force, wake-induced force, added mass force, buoyancy, drag, and wall repulsive force. Basset force is known to be negligible for the bubble which diameter is larger than 1mm (Chen et al., 2022), so we did not take Basset force into consideration in this analysis. Various previous researches suggest numerous approximations and assumptions to the wall repulsive force term, but in this study we will follow Barbosa's method that relates the wall repulsive force with the inertial wake

first (Barbosa et al., 2016), and will develop our original approach to supplement discussion. Therefore, wake-induced force, added mass force, surface tension force, buoyancy, drag force, wall repulsive force can be expressed as

$$F_w \approx \rho_l U r_{eq}^2 u_l \quad (3.2)$$

$$F_{AM} \approx \rho_l d_{eq}^3 a_l \quad (3.3)$$

$$F_\sigma \approx \sigma \Delta A_{eq}/d_{eq} \quad (3.4)$$

$$F_B \approx \rho_l d_{eq}^3 g \quad (3.5)$$

$$F_D \approx \rho_l A_{eq} U^2 C_D \quad (3.6)$$

$$F_R \approx \rho_l d_{eq}^2 U^2 \quad (3.7)$$

respectively. In these equation, each symbol denotes physical properties of the bubble and the liquid: ρ_l, u_l, a_l is density, velocity, acceleration of the surrounding liquid, σ is surface tension coefficient between the liquid and the gas, A_{eq} is surface area calculated from the bubble equivalent diameter, g is gravity constant ($9.8kg \cdot m/s^2$), C_D is the drag coefficient of the bubble. We used an approach of Moore (Moore and Thompson, 1990) to calculate the drag coefficient of the shape and aspect ratio varying bubble. Using properties of 25℃ water and air, wake-induced force and added mass force were calculated to have an order 10^{-5} newtons, while other forces have an order of 10^{-4} newton. So we will neglect wake-induced force and added mass force, and consider only surface tension force, buoyancy, drag force, wall repulsive force in analysis process (Jeong & Park, 2015; Ellingsen & Risso, 2001; Mougin & Magnaudet, 2006; Zawala et al., 2007; Zaruba et al., 2007; Barbosa et al., 2016).

Among these, the forces that acts in wall perpendicular direction

at the moment of collision are only accountable for transition mechanisms. They are buoyancy of the bubble, which makes the bubble to attach to the wall, and the wall repulsive force that makes the bubble move away from the wall. Since no volume of air is lost or gained during the rise of the bubble, buoyancy of the bubble must remain as constant value. Surface tension force acts in a direction that minimizes the surface area of the bubble, so it is reasonable to assume that the major direction of action during the collision is the opposite direction of the wall perpendicular direction, or in a direction that makes the bubble move away from the wall since the bubble flattens to the wall parallel direction before collision. Previous studies usually argued that surface tension term is negligible compared to others, but the need for considering surface tension in force analysis is made obvious by our experimental results, such as observation of vigorous shape deformation after the initial energy-dissipating collisions. Therefore, our transition criterion is slightly modified compared to previous studies. Transition will occur when the wall-perpendicular component of buoyancy is larger than sum of surface tension force and wall repulsive force. So, by balancing terms that act perpendicular to the wall, we can get equations as follows.

$$F_R + F_\sigma \geqq F_B \cos\theta \tag{3.8}$$

$$\rho_l U^2 d_{eq}^2 + \sigma d_{eq} \geqq \rho_l d_{eq}^3 g \cos\theta \tag{3.9}$$

For bubbles with large Weber numbers (We > 1.5), it is known that it is possible to match the parallel component of buoyancy with inertial drag (Barbosa et al., 2016). This would led to

$$F_B \sin\theta \approx \rho_l d_{eq}^3 g \sin\theta \approx \rho_l U^2 d_{eq}^2 \tag{3.10}$$

$$\rho_l d_{eq}^3 g \sin\theta + \sigma d_{eq} \geqq \rho_l d_{eq}^3 g \cos\theta \qquad (3.11)$$

$$\sin\theta + (\frac{\sigma}{\rho g d_{eq}^2}) \geqq \cos\theta \qquad (3.12)$$

where $\frac{\sigma}{\rho g d_{eq}^2}$ term in (3.12) denotes the effect of surface tension on the dynamics of the bubble. However, since this term is comparably smaller (in order of 10^{-2}) than trigonometric function values such as $\sin\theta$, so this force balance equation will predict that the transition will occur near , which is a merely a follow up to previous studies. However, when flattening of the bubble bouncing happens, pressure gradient arouses from the thin liquid film between the bubble and the wall, and it has substantial repulsion effect on the bubble (Podvin et al, 2008). In addition, by looking at the liquid flow field near the wall before and after the transition, we can see that the inertial wake structure is totally different for sliding and bouncing bubbles. In sliding regime, which are cases for the wall inclination angle being smaller than the transition angle, vortex pair is suppressed to the gravitational direction due to the presence of the wall, and that interaction between the wall and the vortex wake structure provides wall repulsive force [Figure 3.6. (a)]. However, in bouncing regime, vortex wake structure behind the bubble is not suppressed in downward direction by the wall anymore, since the inclination angle of the wall has increased enough to have large difference with the gravitational direction and the contact time with the wall and top surface of the bubble is smaller [Figure 3.6. (b)]. Instead, repulsive force is exerted directly by collisions. Therefore, it can be argued that matching wall repulsive force with inertial wake is not valid in bouncing regime. Force balance equation should not only consider the instant of collision, but also consider appropriate time interval before

the collision. In this case, we will scale wall repulsive force using film theory

$$F_R \approx \sigma(\frac{2}{R_{eq}} - (\frac{1}{R_{maj}} + \frac{1}{R_{\min}})2\pi d_{eq}^2 \qquad (3.13)$$

(Klaseboer et al., 2001). Also, since we are looking at time intervals, not instants, drag forces that are acting perpendicular to the wall must be considered, and we used the assumption of C_D from Moore, 1965. (Moore, 1965) Taking all of these into consideration, we can plot the values of forces acting on the bubble frame by frame, and the results are drawn in [Figure 3.7. (a), (b)]. The scaling comparison between these forces shows that as the bubble rises and the distance between the bubble centroid and the wall decreases, total repulsive force acted by the wall increases. The moment when the repulsive force seems to be the local negative peak is the moment when the distance between the wall and the bubble is minimum, i.e., the bubble and the wall begin to collide. In sliding regime, initial collisions push the bubble strongly away the wall, but after sufficient energy dissipation has occurred, the steady-sliding state is achieved, and it is approved by the force diagram. Net upward force perpendicular to the wall direction is steadily positive at steady sliding state [Figure 3.7. (a)]. However, in bouncing regime, strong wall repulsive forces, acted by various sources like thin film pressure and drag, always pushes the bubble away from the wall, as seen as net upward force perpendicular to the wall direction being always negative at the force diagram [Figure 3.7. (b)].

3.4. Energy method

Since shape oscillation through surface tension is a major mechanism for dissipating kinetic energy of bubbles during collision, we have conducted an energy analysis to explain this phenomena using total energy of the bubble. The sum of the kinetic energy and surface tension energy of the bubble is defined as total energy, and the state of the bubble one frame before the collision is defined as near-wall position. By comparing the total energy values between the two near-wall positions, it is able to quantify the dissipation of energy during collisions and the increase and recovery of energy by buoyancy. Each energy values, kinetic energy and surface tension energy, of the bubble can be calculated from the kinematic properties of the bubble at certain frame and expressed as (Jeong and Park, 2015)

$$E_k = \frac{\pi}{12}(\rho_g + c_m \rho_l) d_{eq}^3 (u^2 + v^2) \tag{3.14}$$

$$E_s = \sigma \frac{\pi d_{eq}^2}{2}\left(1 + \frac{1-e^2}{e}\tanh^{-1} e\right) \tag{3.15}$$

$$e = 1 - 1/\chi^2 \tag{3.16}$$

$$c_m = \frac{\alpha}{2-\alpha} \tag{3.17}$$

$$\alpha = \frac{2\chi^2}{\chi^2 - 1}\left(1 - \frac{1}{\sqrt{\chi^2 - 1}}\cos^{-1}(1/\chi)\right) \tag{3.18}$$

$$E_T = E_k + E_s \tag{3.19}$$

where c_m denotes added mass coefficient and can be calculated through (3.17) and (3.18) (Milne-Thomson et al., 1968). Energy analysis results for PMMA wall at different degrees are shown in the

[Figure 3.8. (a), (b), (c)]. When a bubble is beginning to collide with the wall, kinetic energy it gained from free rise turns and accumulates in the form of surface tension energy (flattening), and this leads to the local peak of total energy value before the collision for all cases of our experiments. Then, energy of the bubble is dissipated by shape oscillation in the process of collision, which can be seen by drop of the total and surface tension energy value. Subsequently, the bubble rises again under the force of buoyancy, recovering some or all of its kinetic energy value.

At sliding regimes, initial collisions increase total energy value of the bubble, since violent action-reaction acted by the wall gives momentum to the bubble. Most of the total energy is stored in a form of surface tension energy, lowering the ratio of kinetic energy to the total energy. After reaching steady sliding state, suppressed bubble accumulates its kinetic energy as a form of surface tension energy, and retains its value while sliding because there is no mean to dissipate its energy once steady state is reached and no net force is acted to the bubble [Figure 3.8. (a)].

However, at bouncing regimes, total energy of the bubble is periodically changing with a constant pattern. Depending on the inclination angle of the wall, total energy level either return to the same level as the value before the first collision(free rise) or to the level that reached equilibrium [Figure 3.8. (b), (c)]. Based on these observations, it can be said that the periodicity is shown in the case of dissipated and recovered values were balanced.

Angle	C1	C2	C3	C4
45	0.159	6.840	1.858	0.664
50	0.196	7.476	0.668	0.696
55	0.251	7.871	2.312	0.775
60	0.282	8.586	1.636	0.762
65	0.310	9.006	2.576	0.698
70	0.593	12.585	0.718	1.065
75	0.677	12.552	0.728	1.157
80	0.802	15.230	0.816	1.391
85	1.045	17.824	3.472	1.619

Table 3.1. Constants of sine fitted equations, PMMA wall

Angle	C1	C2	C3	C4
45	0.182	6.870	1.275	0.641
50	0.199	7.220	1.426	0.709
55	0.204	7.721	0.723	0.693
60	0.280	8.328	1.570	0.767
65	0.281	8.434	1.631	0.818
70	0.279	9.630	2.970	0.808
75	0.758	13.600	0.716	1.465
80	1.048	14.929	2.754	1.718
85	1.305	16.567	0.740	1.994

Table 3.2. Constants of sine fitted equations, glass wall

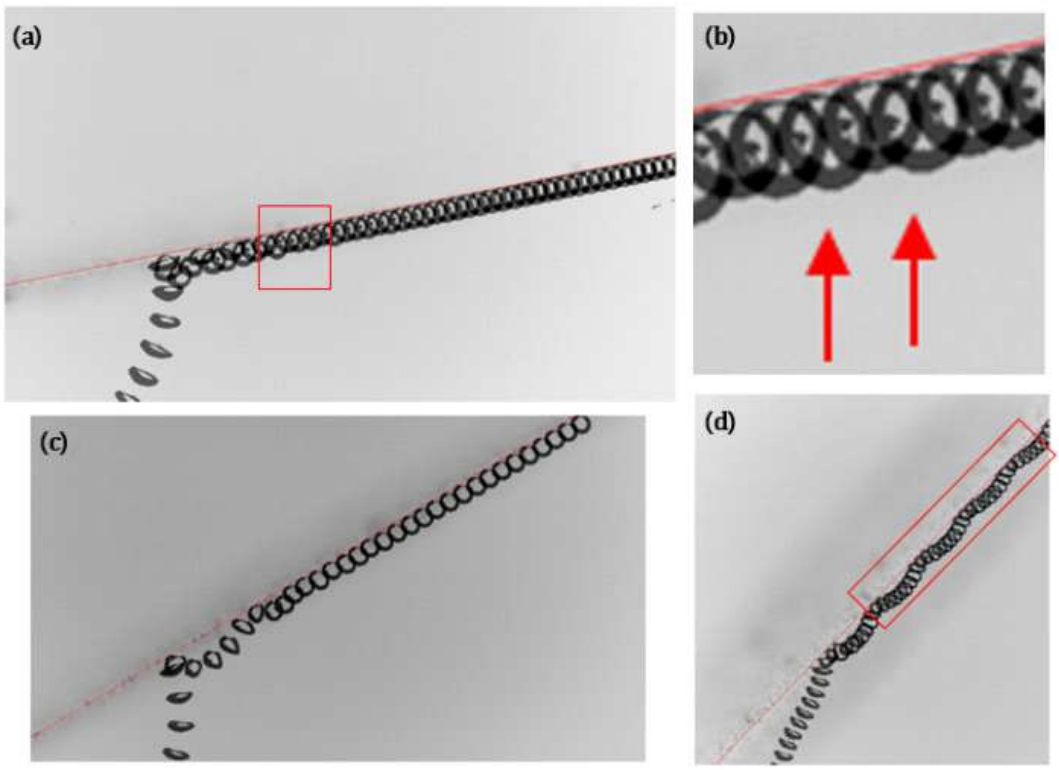

Figure 3.1. Superimposed bubble edge image at the inclination angle of the wall of (a) 10°, (c) 30°, (d) 45° at PMMA wall, (b) Magnified view of red squared area in (a)

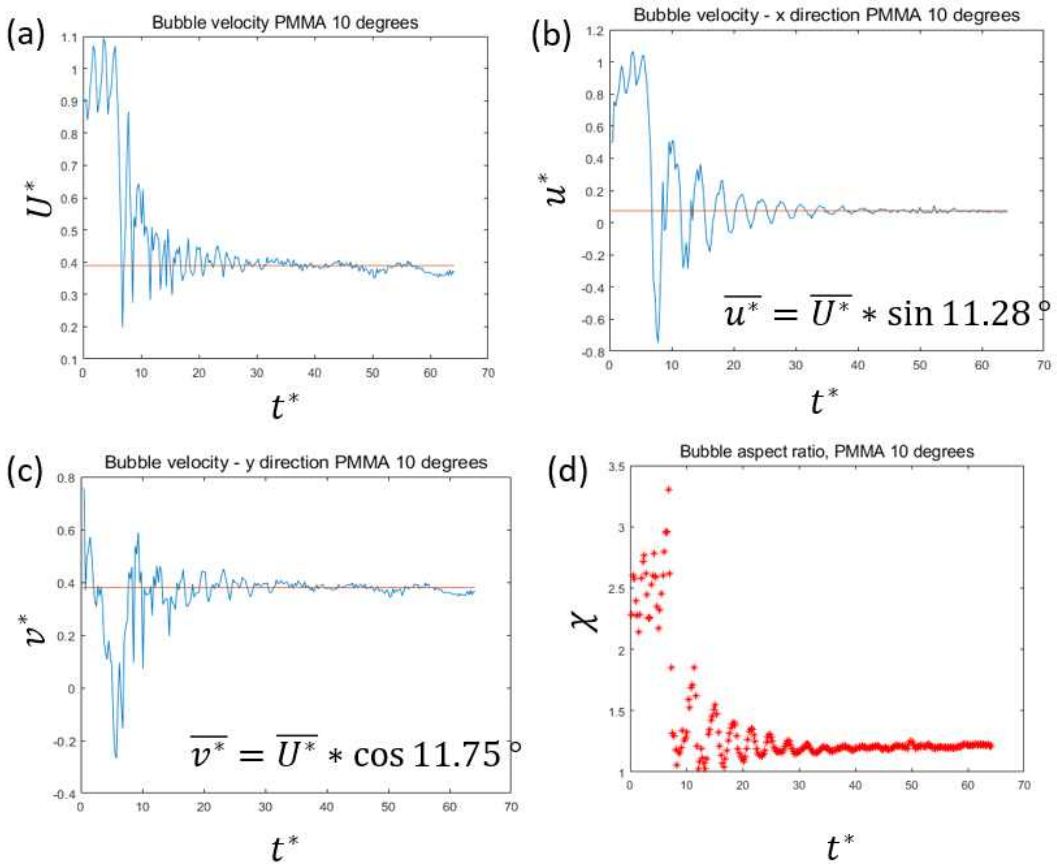

Figure 3.2. (a) Total speed (b) x-directional speed (c) y-directional speed of the bubble centroid at the inclination angle of 10°, PMMA wall (d) Aspect ratio of the bubble at the inclination angle of 10°, PMMA wall

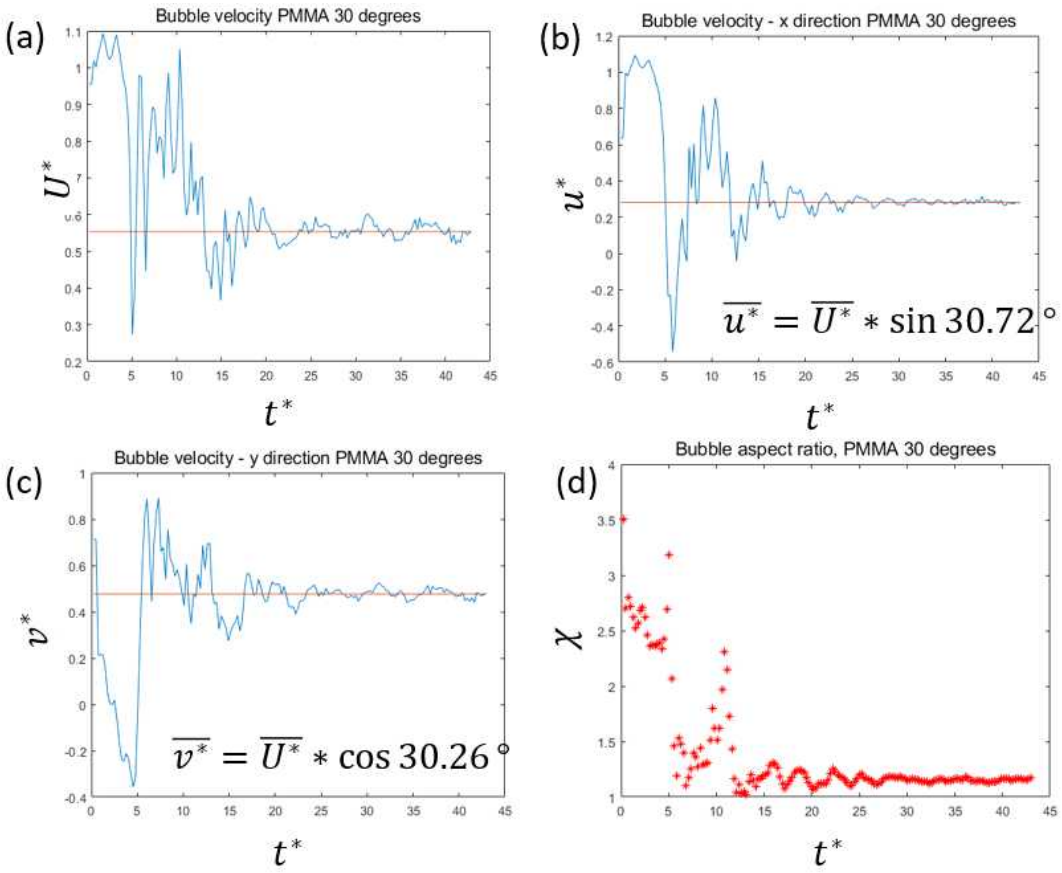

Figure 3.3. (a) Total speed (b) x-directional speed (c) y-directional speed of the bubble centroid at the inclination angle of 30°, PMMA wall (d) Aspect ratio of the bubble at the inclination angle of 30°, PMMA wall

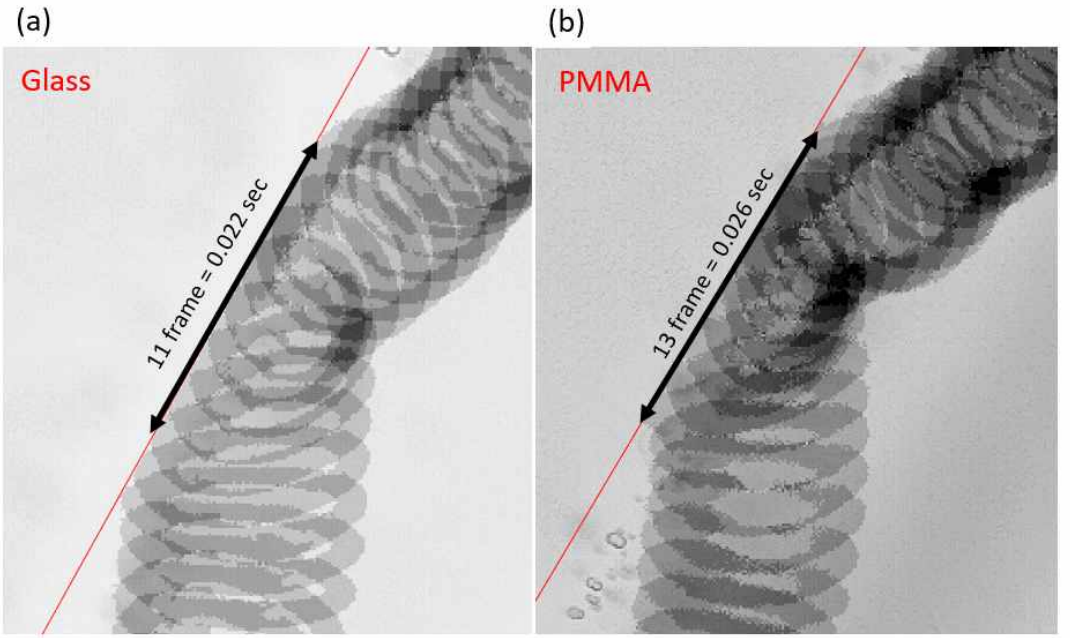

Figure 3.4. Superimposed image of the bubble impacting on the (a) glass (b) PMMA wall, at the inclination angle of the wall of 45°

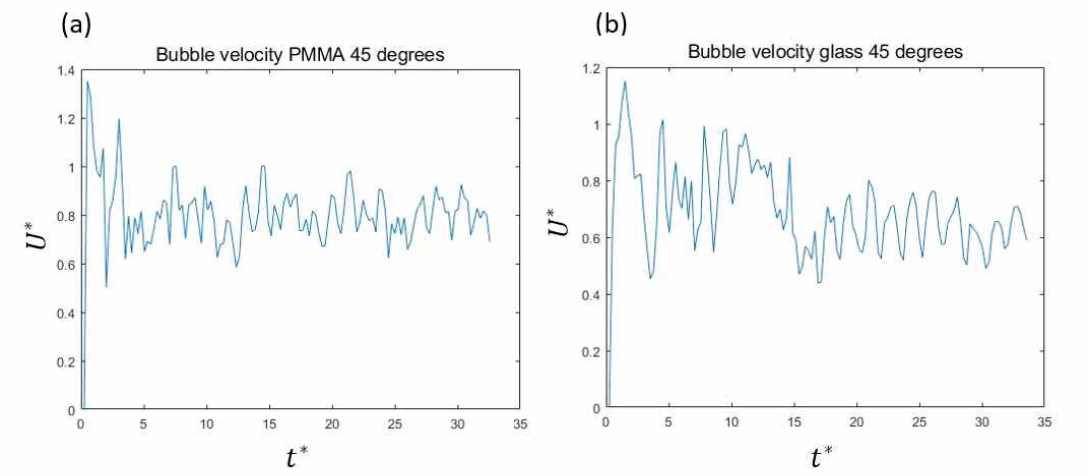

Figure 3.5. Non-dimensionalized velocity of the bubble bouncing with the (a) PMMA (b) glass wall of inclination angle of 45°

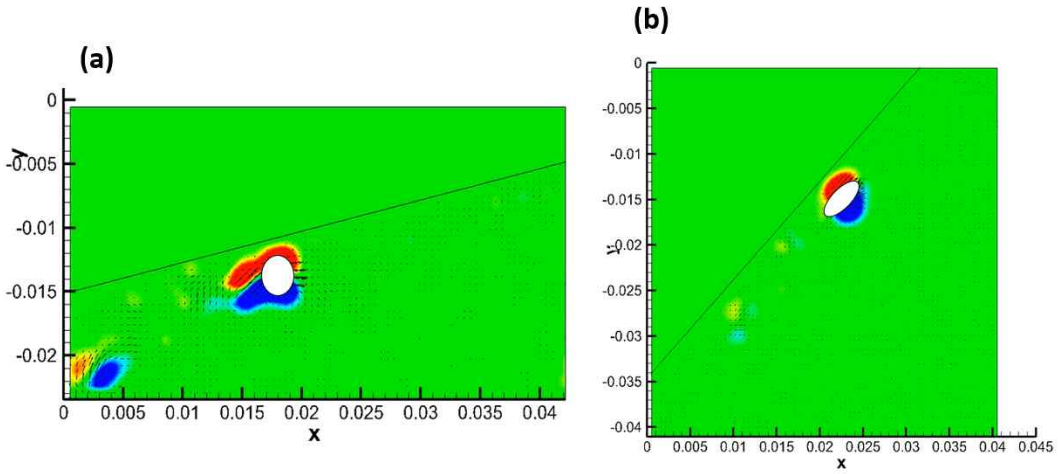

Figure 3.6. Vortex pair structure behind the bubble at the inclination angle of (a) sliding regime (b) bouncing regime

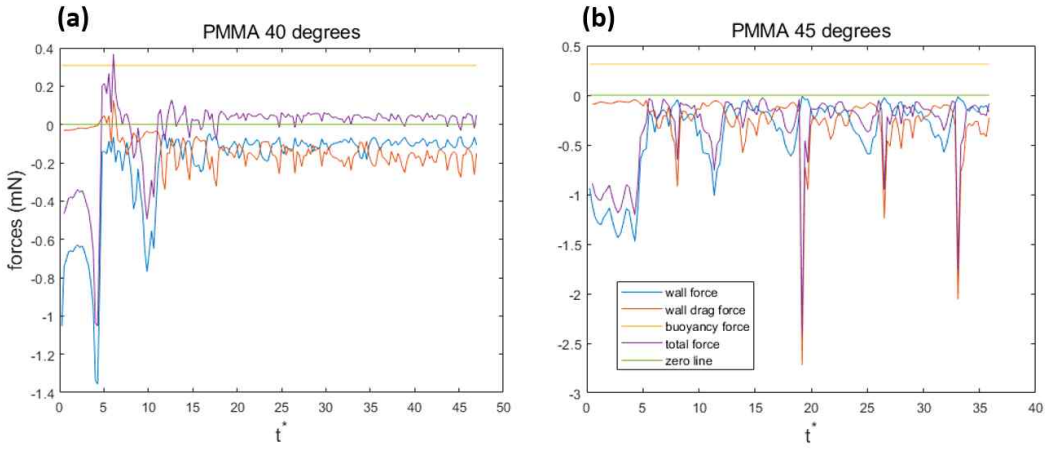

Figure 3.7. Forces that act on the bubble with the inclination angle of (a) 40°, (b) 45° of PMMA wall

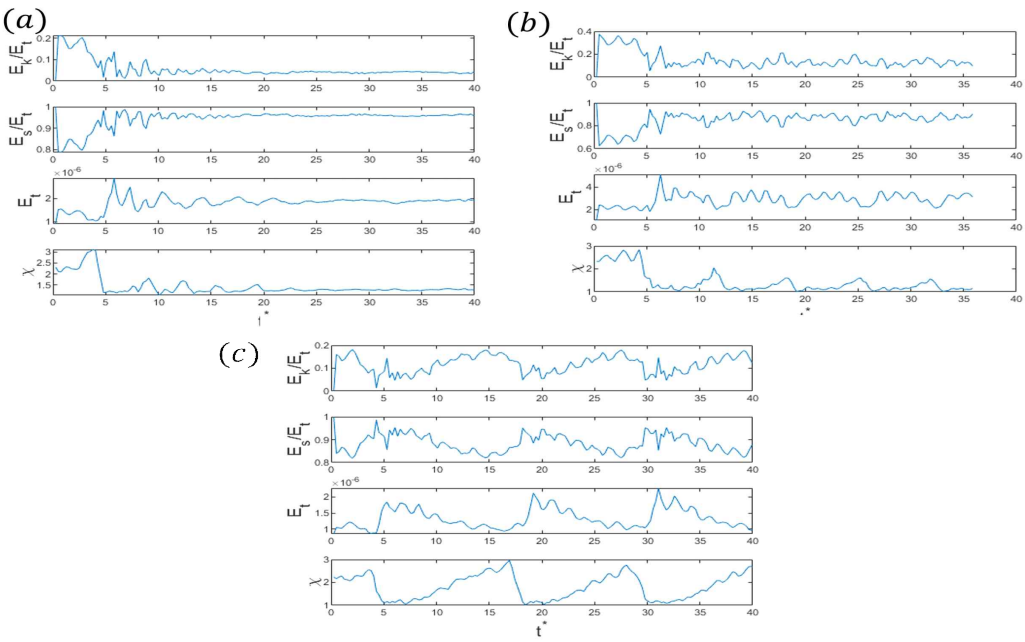

Figure 3.8. Ratio of kinetic energy to total energy value, ratio of surface tensiono energy to total energy value, total energy value, aspect ratio of the bubble at the inclination angle of (a) 20°, (b) 45°, (c) 80° of PMMA wall

Chapter 4.
Conclusions

Behavior of bubbles rising under the influence of the inclined wall can be divided into two major behavior categories: sliding along the wall parallel direction or periodic bouncing against the wall while rising. The transition condition of such behavior is independent of the wall material, but found to be the function of the inclined angle and surface tension of the wall in high Weber and Reynolds number case. Sliding bubble regime can be subdivided by the criterion of occurrence of shape oscillation, which is a phenomena to dissipate residual surface tension energy over accumulated in bubble surface. The wall boundary condition, or the material of the wall, affected the size of wall effective region, which is an area where the effect of the wall is significant, resulting in different bubble trajectory and bubble dynamics for high inclination angle of the wall. Bouncing regime can be subdivided into two sub-regime by whether the bubble escapes from the wall effective region or not. Wettability of the wall also affected the contact time between the bubble and the wall, but it had little effect on kinematic property of the bubble. During the collision with the wall, kinetic energy of the bubble which it gained from the buoyancy is interchanged into the form of surface tension energy and dissipated during the process of deformation and restitution of surface area.. This classification and detailed explanation about the transition mechanism have led to a profound understanding of the bubble dynamics and the bubble-surface interactions. Further research exploring detailed mechanisms regarding shape oscillation modes, coefficient of restitution, and researches about wall effects for various

compositions such as superhydrophobic or superhydrophilic walls are recommended.

Bibilography

Barbosa, C., Legendre, D. and Zenit, R., 2016. Conditions for the sliding-bouncing transition for the interaction of a bubble with an inclined wall. *Physical Review Fluids*, **1(3)**. 032201.

Barbosa, C., Legendre, D. and Zenit, R., 2019. Sliding motion of a bubble against an inclined wall from moderate to high bubble Reynolds number. *Physical Review Fluids,* **4(4)**. 043602.

Chen, H., Ding, W., Wei, H., Saxén, H. and Yu, Y., 2022. A coupled CFD-DEM study on the effect of Basset force aimed at the motion of a single bubble. *Materials,* **15(15).** 5461.

Ellingsen, K. and Risso, F., 2001. On the rise of an ellipsoidal bubble in water: oscillatory paths and liquid-induced velocity. *Journal of Fluid Mechanics*, **440.** 235-268.

Haberman, W.L. and Morton, R.K., 1953. An experimental investigation of the drag and shape of air bubbles rising in various liquids. David Taylor Model Basin Washington DC.

Hirdaris, S.E., Cheng, Y.F., Shallcross, P., Bonafoux, J., Carlson, D., Prince, B. and Sarris, G.A., 2014. Considerations on the potential use of Nuclear Small Modular Reactor (SMR) technology for merchant marine propulsion. *Ocean Engineering,* **79.** 101-130.

Javadi, K. and Davoudian, S.H., 2018. Surface wettability effect on the rising of a bubble attached to a vertical wall. *International Journal of Multiphase Flow,* **109.** 178-190.

Jeong, H. and Park, H., 2015. Near-wall rising behaviour of a deformable bubble at high Reynolds number. *Journal of Fluid Mechanics,* **771.** 564-594.

Khodadadi, S., Samkhaniani, N., Taleghani, M.H., Gorji-Bandpy, M.

and Ganji, D.D., 2022. Numerical simulation of single bubble motion along inclined walls: A comprehensive map of outcomes. *Ocean Engineering,* **255.** 111478.

Lee, J. and Park, H., 2017. Wake structures behind an oscillating bubble rising close to a vertical wall. *International Journal of Multiphase Flow,* **91.** 225-242.

Lee, J. and Park, H., 2022. Flow induced by the single-bubble chain depending on the bubble release frequency. *Physics of Fluids,* **34(3).** 033312.

Sol, D., Laca, A., Laca, A. and Díaz, M., 2020. Approaching the environmental problem of microplastics: Importance of WWTP treatments. *Science of the Total Environment,* **740.** 140016.

Lindken, R. and Merzkirch, W., 2002. A novel PIV technique for measurements in multiphase flows and its application to two-phase bubbly flows. *Experiments in fluids,* **33(6).** 814-825.

Milne-Thomson, L.M., 1968. Plane elastic systems (Vol. 6). Berlin: Springer-Verlag.

Moore, D.W., 1965. The velocity of rise of distorted gas bubbles in a liquid of small viscosity. *Journal of Fluid Mechanics,* **23(4).** 749-766.

Moore, M., & Thompson, M., 1990. The effects of distance learning: A summary of literature. ERIC Document Reproduction Service No. ED330 321.

Ngai, J.H., Ho, J.K., Chan, R.K., Cheung, S.H., Leung, L.M. and So, S.K., 2017. Growth, characterization, and thin film transistor application of CH 3 NH 3 PbI 3 perovskite on polymeric gate dielectric layers. *Rsc Advances,* **7(78).** 49353-49360.

Mougin, G. and Magnaudet, J., 2006. Wake-induced forces and

torques on a zigzagging/spiralling bubble. *Journal of Fluid Mechanics,* **567.** 185-194.

Winandy, L., Hilpert, F., Schlebusch, O. and Fischer, R., 2018. Comparative analysis of surface coating properties of five hydrophobins from Aspergillus nidulans and Trichoderma reseei. *Scientific reports,* **8(1).** 12033.

Klaseboer, E., Chevaillier, J.P., Maté, A., Masbernat, O. and Gourdon, C., 2001. Model and experiments of a drop impinging on an immersed wall. *Physics of Fluids,* **13(1).** 45-57.

Zaruba, A., Lucas, D., Prasser, H.M. and Höhne, T., 2007. Bubble-wall interactions in a vertical gas–liquid flow: Bouncing, sliding and bubble deformations. *Chemical engineering science,* **62(6).** 1591-1605.

Zawala, J., Krasowska, M., Dabros, T. and Malysa, K., 2007. Influence of bubble kinetic energy on its bouncing during collisions with various interfaces. *The Canadian Journal of Chemical Engineering,* **85(5).** 669-678.

Zhang, H., Ren, X., Luo, C., Tong, Y., Larson, E.A., Lu, Z. and Gu, J., 2019. Study on transient characteristics and influencing of temperature on cavitation bubbles in various environments. *Optik,* **187.** 25-33.

기울어진 벽과 충돌하는 상승 기포 역학에 대한 실험적 연구

최 진 용
기계공학부
서울대학교 대학원

국문 초록

본 연구에서는 실온의 수돗물로 채워진 아크릴 탱크 위에 설치된 기울어진 벽의 영향을 받는 단일 상승 기포의 역학을 실험적으로 조사하고 분석하였다. 기포는 2-3mm 범위의 등가 직경을 가지는 2차원 타원체 모양을 가지고 있으며, 이 기포를 다양한 재료(PMMA 및 유리)와 기울어진 각도가 5도 간격으로 5도에서 85도까지 변하는 벽에 충돌시킴으로서 실험을 수행했다. 본 연구에서는 섀도우그래피 기법을 이용하여 기포의 궤적과 기포 표면의 형상 변형을 측정하였고, 고속 이상 입자 영상 속도계를 이용하여 벽 근처의 액체 유동장의 변화를 관찰하였다. 벽과 처음 충돌한 후 가포는 벽과 평행하게 미끄러지거나 벽에 반복적으로 튕겨 나온다는 것이 관찰되었다. 충돌 순간 기포에 작용하는 벽 수직 방향과 벽 평행 방향 힘의 값을 비교하여 기포 역학의 전이 메커니즘을 설명하였고, 이를 통해 높은 Weber 수에서 기포 움직임의 전이 조건은 벽 경계 조건에 관계없이 벽의 기울어진 각도에 의해서만 결정된다는 것을 확인하였다. 이러한 전이는 주로 벽 근처의 얇은 액체막과 변형된 기포 사이의 압력 차이에 의해 발생하는 벽

반발력이 벽 인력으로 작용하는 기포의 부력과 균형을 이룰 때 발생한다. 이전 연구에서 일반적으로 무시할 수 있는 것으로 여겨졌던 표면장력은 기포를 벽에서 멀어지는 방향으로 작용하며, 전이 조건에 변화를 줌을 확인할 수 있다. 기포 궤적을 삼각 방정식으로 나타내어 주기와 진폭의 변화를 관찰하여 벽의 젖음성의 효과에 대해 알아보았는데, 벽 경계 조건의 효과는 벽의 경사각이 전이 각보다 훨씬 높을 때만 영향을 주었다. 또한 전이가 발생하기 전과 발생한 후의 기포-벽 상호 작용 메커니즘은 서로 다른 양상으로 나타났는데, 기포 주변의 액체 유동장의 시간에 따른 변화를 통해 이를 살펴볼 수 있었다. 이를 이용하여 우리는 산업 응용 분야에서 다상유동을 이용하는 것의 효과를 제안할 수 있었다.

주요어 : 상승기포, 젖음성, 섀도우그래피, 고속 입자 이상 속도계, 표면장력.
학번 : 2021-22293